Connecting complex and simplified models of tipping elements: a nonlinear two-forcing emulator for the Atlantic meridional overturning circulation

[version 1; peer review: 1 approved, 1 approved with reservations]

Amaury Laridon[a12]

Conceptualization

Data Curation

Formal Analysis

Funding Acquisition

Investigation

Methodology

Project Administration

Software

Supervision

Validation

Visualization

Writing – Original Draft Preparation

Writing – Review & Editing

URI: https://orcid.org/0009-0009-6559-9249

, Victor Couplet[2]

Conceptualization

Formal Analysis

Methodology

Project Administration

Resources

Software

Supervision

Writing – Review & Editing

, Justin Gérard[2]

Resources

Writing – Review & Editing

, Wim Thiery[1]

Project Administration

Supervision

Writing – Review & Editing

URI: https://orcid.org/0000-0002-5183-6145

, Michel Crucifix[2]

Conceptualization

Project Administration

Supervision

Writing – Review & Editing

[1] Water and Climate, Vrije Universiteit Brussel, Brussels, Brussels, 1050, Belgium

[2] Earth and Life Institute, Universite catholique de Louvain, Louvain-la-Neuve, Walloon Region, 1348, Belgium

Author notes:

Correspondence to: [a] Amaury.Laridon@vub.be

Abstract

Background

Despite its far-reaching implications, accurately characterizing the non-linear dynamics of the Atlantic Meridional Overturning Circulation (AMOC) remains a significant challenge. Complex models, including Earth System Models (ESMs) and Earth System Models of Intermediate Complexity (EMICs), offer valuable insights; however, they are computationally expensive and subject to substantial uncertainties in identifying AMOC tipping points. In contrast, simple conceptual models based on simple dynamical systems have been developed to represent tipping elements such as the AMOC. These models can be calibrated against complex models to explore various scenarios and forcing spaces, functioning as emulators. Traditionally, such emulators have focused on a single forcing variable, typically global mean temperature, despite the well-established influence of freshwater fluxes on AMOC dynamics. Moreover, existing two-forcing AMOC emulators lack robust calibration methods against complex models.

Methods

In this study, we develop and validate a two-forcing AMOC emulator that incorporates global mean temperature and freshwater flux, grounded in non-linear dynamics. The emulator is calibrated against the AMOC response within the EMIC cGENIE. After validation, the emulator is integrated into SURFER, a reduced-complexity climate model, enabling rapid simulation of AMOC trajectories under diverse emission scenarios.

Results

By accounting for Greenland Ice Sheet melt, the emulator captures three additional collapse trajectories for emission scenarios ranging from SSP3-7.0 to SSP5-8.5. Furthermore, the emulator allows an assessment of the critical forcing manifold of the AMOC in the complex model, enabling the identification of combined forcing thresholds for the AMOC and serving as a tool for comparing the sensitivities of complex models.

Conclusions

With its low computational cost and calibration accuracy, our emulator offers an efficient tool for exploring AMOC dynamics in future climatic scenarios. Finally, the methods used to develop this emulator are generalizable, providing a framework for studying other tipping elements in research.

Plain Language Summary

As global temperatures rise due to greenhouse gas emissions, certain key components of the Earth's climate system are approaching critical thresholds known as tipping points, beyond which large, potentially irreversible changes may occur. One such tipping element is the Atlantic Meridional Overturning Circulation (AMOC), a crucial ocean current responsible for redistributing heat between the hemispheres. If the AMOC were to collapse, it could result in substantial regional changes in temperature, precipitation, and other critical aspects of the climate. However, the exact location of the AMOC tipping point and the time it would take to collapse remain uncertain. Complex models remain uncertain, and running them is computationally expensive, making it difficult to explore a wide range of potential future scenarios. In this study, we developed an emulator—a simplified conceptual model calibrated on a more complex model—to reproduce the behaviour of the AMOC during a potential collapse. This emulator is built on a new methodology that improves the alignment between simplified dynamics and complex models. The resulting tool enables the production of numerous AMOC simulations under various emission scenarios with low computational cost, while remaining consistent with our understanding of the physical processes that govern the AMOC. We present simulations, with this emulator, showing AMOC collapse under future high emission pathways. This emulator and methods enable researchers to better explore the potential responses of the AMOC to future emissions and strengthens our ability to predict and prepare for abrupt changes in the climate system.

Keywords

Climate change, Tipping Points, AMOC, Emulator, Non-linear dynamics, SURFER, cGENIE

1. Introduction

1.1 The AMOC as a Tipping Element: Addressing High Uncertainties

The Atlantic Meridional Overturning Circulation (AMOC) is a key component of the climate system. It plays a central role in the transport of heat and salt throughout the global ocean and significantly influences both regional and global climate (1–3). The AMOC has been identified as a tipping element, a large-scale component of the climate system that can reach a tipping point (4). A tipping point refers to a critical threshold in a forcing parameter, known as the bifurcation parameter, beyond which a small perturbation of this parameter can cause the tipping element to transition from one equilibrium state to another, resulting in a qualitative change (4). For the AMOC, the secondary stable equilibrium corresponds to a collapsed state, in which the overturning circulation ceases (5). A cessation or even a slowdown of the AMOC would have significant consequences for temperatures in the North Atlantic (3–6), as well as impacts on the carbon cycle (7), monsoons (2), and, potentially, other tipping elements (5,8,9).

Accurately simulating the AMOC requires an understanding of its physical dynamics. The AMOC operates through the sinking of large amounts of salty water originating from the South Atlantic. As the water travels northward, it cools and becomes sufficiently dense to sink into the depths, forming the North Atlantic Deep Water (NADW). This water mass then returns to the South Atlantic through the deep layers of the Atlantic Ocean (10,11). The AMOC is a component of the so-called thermohaline circulation, as it is driven by density differences determined by the temperature and salinity of the water. The tipping point of the AMOC corresponds to a critical threshold in the stratification of North Atlantic waters, beyond which further stratification becomes self-amplifying. With global warming, the increase in Atlantic water temperature reduces its density, thereby increasing its buoyancy (12). This thermal forcing is the dominant mechanism driving AMOC weakening (13–15). The second forcing mechanism involves a disturbance in the salinity of the water within the Atlantic. As the Greenland Ice Sheet (GIS) melts due to global warming, large quantities of freshwater are added to the deep-water sinking regions in the North Atlantic. This freshwater flux reduces the water's density, increasing its buoyancy and diminishing its ability to sink into the depths, thereby weakening the intensity of the AMOC (16–18). Future variations in water salinity in the North Atlantic may also result from changes in the precipitation-evaporation (P-E) balance driven by temperature anomalies (19). The theory predicts critical threshold of water stratification that, if exceeded for a prolonged period, can become self-sustaining, as the AMOC can no longer transport warm and salty water to the North Atlantic (20), ultimately leading to the collapse of the circulation (5,16,21). Once reached, this collapse state is irreversible, as returning to the critical value of the bifurcation parameter will not allow the system to return to its initial equilibrium. A characteristic hysteresis phenomenon is thus present, preventing a return to the initial state within timescales relevant to human lifetimes (4,22).

There is evidence that the AMOC has slowed during the 20th century (23), with reconstructions indicating a 15% decline over the past 70 years (24), bringing it closer to its tipping point. However, observations of AMOC slowdown are subject to considerable uncertainty (25), and although the AMOC may have collapsed in the past (8,26,27), accurately forecasting its future evolution (i.e. when and at what rate it may collapse) remains a significant challenge (5,28,29). Estimates of the tipping point for the AMOC must therefore rely on models, but the results vary significantly (29). Some studies place the tipping point at a global mean temperature anomaly of 8°C, while others suggest it may already be as low as 1.4°C (30). Consequently, some studies estimate that a complete collapse of the AMOC could occur by the end of this century (31), or not until 2300 (16). In addition, there is also sensitivity to the rate of the applied forcing (32,33). Lastly, the tipping dynamics of the AMOC cannot be fully understood without considering those of the GIS, which has a melting threshold beyond which its decline becomes irreversible (30). In addition to the destabilizing effect of GIS melting on the AMOC due to freshwater input, a collapse of the AMOC would, conversely, have a stabilizing effect on the GIS. Indeed, the

resulting regional cooling following an AMOC shutdown would slow down the melting of the GIS. Thus, a coupling between the AMOC and the GIS exists, potentially giving rise to tipping cascades (34). In this situation the collapse of one system triggers the failure of another or, conversely, helps stabilize it (35). Again, significant uncertainties remain in the projections of these dynamics, particularly due to the uncertainty regarding the future of the AMOC (5).

1.2 The Need for Simplified Models Capturing First-Order Dynamics

This significant uncertainty regarding the future evolution of AMOC collapse stems from the diversity of models and approaches employed. To assess the stability of the AMOC, stability diagrams are constructed using hysteresis experiments, in which the forcing is slowly varied along a back-and-forth scenario. Such simulation are possible with state-of-the-art Earth System Models (ESMs) (6), but they remain extremely challenging due to their prohibitive computational demands. As a result, ESMs are generally unable to simulate a large number of full AMOC hysteresis curves (36). Consequently, Earth System Models of Intermediate Complexity (EMICs) offer a better compromise between explicitly resolving processes and computational efficiency for generating AMOC hysteresis curves (28,37). Like the more complex models, EMICs exhibit significant variability in the location of the tipping point and, in their projections of the future evolution of the AMOC (28). However, with current computer technology, even EMICs appear too expensive to efficiently exploring the range of potential forcing scenarios and their associated AMOC responses. The possibility must also be considered that most models, EMICs and ESMs included, exhibit excessive stability due to biases in ocean salinity distribution (38,39). This explains a sustained interest for conceptual models to explore uncertainties and fundamental aspects of tipping points and tipping cascades (35,40–42).

This approach primarily relies on modelling the dynamics of tipping elements through a double-fold bifurcation structure (40–43), consistent with theory, and also supported by real world measures of stability indicators suggesting that AMOC resides in a bistable regime(44–46). The ocean circulation system is then modelled possessing two stable equilibria separated by an unstable equilibrium. When the bifurcation parameter reaches the critical value of the tipping point, the system can transition from its initial stable equilibrium to the second. These models mathematically impose that the AMOC behaves as a nonlinear dynamical system with this specific double-fold structure, thereby defining its intrinsic tipping element dynamics. The primary advantage of this approach, beyond its ability to capture the hypothesized dynamical behaviour in general terms, lies in its computational efficiency. By calibrating the simplified dynamics on the output of more complex models, we create what is known in the field as an “emulator,” while the complex model is referred to as the “simulator” (47). When these tipping element emulators are coupled with a reduced-complexity climate model, they offer a tool that is both process-based and computationally efficient, adequate to study evolution over several millennia driven by realistic concentration or emissions scenarios (40).

1.3 Challenges in Designing a Two-Forcing Emulator

An emulator based on the concept of a double-fold bifurcation was introduced by Martinez Montero et al. (48) within the reduced-complexity climate model SURFER v2.0. to simulate the dynamics of ice sheets. This emulator considers only a single forcing variable, specifically the temperature anomaly computed from emission scenarios. Couplet et al. (40,49), further developed SURFER (v3.0) by allowing for the coupling of tipping elements and hence the inclusion of an additional forcing variable. The challenge, however, lies in the calibration technique for the model parameters, which must use existing literature and additional simulations with complex models. Couplet et al. (40) sampled the tipping element parameters from uniform distributions spanning the range of values reported in the literature. In contrast to Couplet et al. (40), our approach focuses on calibrating the parameters of a two-parameter physical forcing emulator to align with any given hysteresis curve from a simulator. To our knowledge, this methodology is novel. It enables a more realistic calibration of the emulator while facilitating the systematic exploration of the forcing space across different emission scenarios across multimillennial timescales. Importantly, it preserves the key characteristics of the emulated simulator, allowing for computationally efficient yet physically consistent simulations.

Therefore, this study seeks to address the following objective of developing an AMOC emulator with two forcing parameters — temperature and freshwater flux — that can be calibrated against hysteresis from simulators and integrated into a climate model. To assess the emulator's performance, we consider three key criteria: (i) its ability to correctly predict whether a collapse occurs in the target simulator, (ii) its ability to reproduce the timing of such a collapse, and (iii) its skill in predicting an AMOC collapse under the combined influence of temperature and freshwater flux, as represented in the simulator. The paper is structured as follows. In Section 2, we introduce the AMOC Tipping Calibration Module (ATCM), a simplified nonlinear dynamical model based on the double-fold bifurcation structure with two forcing parameters: temperature anomaly and freshwater flux. We also describe the calibration module used to fit the double-fold structure to any hysteresis curve derived from a simulator. This novel module is based on the assumption of independent forcing calibration experiments, which allows for a generalization of the method by Martinez Monteiro et al. (48). In Section 3, we apply this calibration process to cGENIE, an EMIC, using three calibration experiments. We then validate the ATCM as an emulator by comparing its results with those from four additional cGENIE experiments. Subsequently, we integrate the ATCM into the SURFER climate model, creating a new configuration that provides a calibrated emulator of the AMOC within a fast climate model. This tool facilitates further investigation of the potential collapse dynamics of the AMOC under realistic emission scenarios. It also allows an assessment of the linear critical manifold of the simulator. Section 4 presents our key findings and discusses the limitations of our approach. Additionally, the section outlines how our methods can be applied to emulate other tipping elements, as well as to couple the impact of an AMOC collapse on GIS dynamics, thereby enabling a tipping cascade emulator. We present our conclusions in Section 5.

2. Methods

We introduce the AMOC Tipping Calibration Module (ATCM), an emulator designed to represent the tipping dynamics of the AMOC under two forcing parameters. The key feature of this emulator is its ability to calibrate simplified AMOC dynamics to match any hysteresis curve derived from a more complex, process-based model. We detail the equations that define the model and describe the methodology used for its calibration. The AMOC model is based on the normal form of a double-fold bifurcation, which has been demonstrated in previous studies to be effective in modelling the tipping element behaviour of the AMOC (40,42). The calibration technique is built upon the ice sheet emulator implemented in SURFER v2.0 (48) and incorporates the assumption of independent forcing in the calibration experiments. Subsequently, in the results section, the ATCM is calibrated on the cGENIE model, enabling it to act as an emulator for the AMOC.

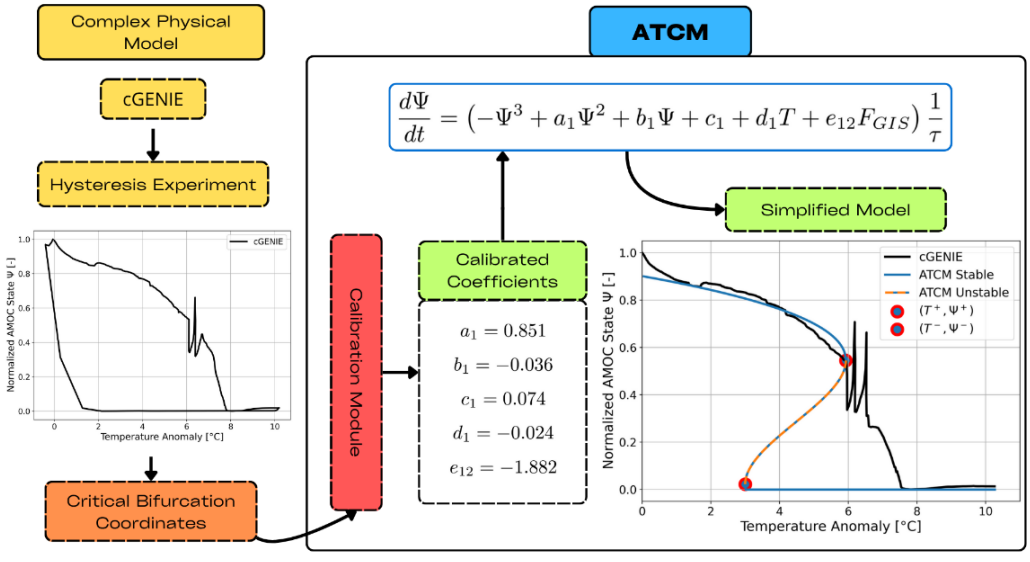

Figure 1 : Schematic of the AMOC Tipping Calibration Module (ATCM). The module requires input in the form of bifurcation coordinates derived from complex experiments. These coordinates are used to adjust the calibration coefficients within the simplified tipping element model.

2.1 AMOC Dynamical Model

The overall scheme of the ATCM is depicted in Figure 1. The non linear ordinary differential equation that describes the AMOC intensity is given by,

$$\frac{d\Psi}{dt}(\Psi, T, F_{GIS}) = \left(\overbrace{-\Psi^3 + a_1\Psi^2 + b_1\Psi + c_1}^{internal\ dynamics} + \underbrace{d_1 T + e_{12} F_{GIS}}_{forcings} \right) \frac{1}{\tau}, \quad (1)$$

This equation is derived from the normal form of a double-fold bifurcation, enabling the representation of the first-order tipping dynamics of the AMOC. Consequently, the tipping element model acts as a generic dynamical system designed to function as an emulator. The use of a generalized normal form of a double-fold bifurcation is a parsimonious and effective approach to capture bi-stability and hysteresis generally associated with tipping elements in the climate system (40,42,48). The state variable Ψ is dimensionless and spans the interval [0,1], defining the state of the AMOC relative to its pre-industrial level $\Psi(t = 0) = 1$. For the AMOC, Ψ is the ratio of its current intensity in Sv with its pre-industrial value. The first group of terms in Eq.(1) represents the internal dynamics of the tipping element. Since it is a cubic polynomial of the state variable it allows the tipping element to have 1,2 or 3 stable states depending on its forcings (40). The coefficients $a_1, b_1, c_1, d_1, e_{12}$ do not correspond directly to specific physical properties, but they control the positions of the bifurcation points and can be calibrated based on hysteresis experiments diagnosed in the simulators. Finally, the parameter τ represents an inverse time scale characterizing the typical duration required for the system to deviate from its equilibrium states. In other words, it quantifies the characteristic timescale of AMOC adjustment following a perturbation. It can be calibrated based on a transient experiment from the simulator and constitutes the final parameter of our emulator.

The first forcing term, T, which appears in Eq.(1), represents the global mean surface air temperature anomaly relative to pre-industrial levels and encapsulates the physical effects of warming on AMOC water stratification. The second forcing term, F_{GIS}, represents the freshwater flux resulting from GIS melting, which in turn weakens the AMOC by enhancing water column stratification. In the following subsection, we introduce the method to calibrate all parameters of our emulator, $a_1, b_1, c_1, d_1, e_{12}$ and τ, using three calibration experiments derived from the simulator.

2.2 Calibration Module

For the calibration, we aim to find the best fit of our double-fold structure to the complex hysteresis curve, ensuring that our simplified dynamics come as close as possible to the bifurcation points identified in the process-based hysteresis. In the paper describing the SURFER v2.0 model, Martinez-Montero et al.(48) also modelled tipping elements using a canonical double-fold normal form. They developed a method to calibrate the emulator using the coordinates of the bifurcation points identified in the simulator experiments. Martinez-Monteiro et al. (48) compute explicitly the calibration parameters as a function of the coordinates of the tipping point in the forcing space, as the latter are easier to jutify. This method also allows to test the underlying hypothesis that the leading-order dynamics of tipping elements such as the AMOC can be captured by a double-fold. Our objective is to adhere to this calibration strategy. However, the mathematical framework presented by Martinez-Monteiro et al. (48) for modelling each individual ice sheet relies on an ordinary differential equation with only one forcing parameter, namely the temperature anomaly. In our case, for the AMOC, we have two forcing variables: the temperature anomaly and the freshwater flux.

To generalize the method of Martinez-Monteiro et al. (47) we need an operational assumption. Specifically, we assume that the simulator used to calibrate the hysteresis of the AMOC allow for independent application of forcing to the AMOC. In other words, with our emulator, we should be able to access process-based models that can force the AMOC solely through globally averaged atmospheric temperature anomalies while keeping the freshwater flux forcing constant, and vice versa. This is technically feasible with most models. If the aim is also to emulate the transition from the collapsed state to the nominal state, an additional constraint arises in the selection of the simulator. Specifically,

the simulator used as a reference must be adequate for conducting hysteresis experiments, which involve simulations where the tipping element remains in quasi-equilibrium. For instance, in the cGENIE two first experiments used for calibration of collapse dynamics, simulations span over 20,000 years (see Supplementary Materials). This requirement implies that models categorized as EMICs are generally more suitable candidates to provide reference simulations for emulation (36). Throughout the text, we will refer to EMICs as the simulator we aim to emulate, although the emulator can be calibrated using any process-based model of the AMOC.

The procedure for calibrating our simplified bifurcation diagram, which is generalizable to N forcings, is as follows. With N forcing variables, we conduct N independent sensitivity experiments, each designed to separately calibrate the bifurcation diagram corresponding to a specific forcing variable. In each case, the remaining $N-1$ forcing variables are held constant, thereby reducing the calibration to a Martinez-Monteiro et al. (48)-type model involving only a single forcing dimension. For the AMOC, $EXPA$ is defined as the calibration experiment of the AMOC intensity with respect to a temperature forcing in any simulator that satisfies the aforementioned conditions. From this experiment we can retrieve the coordinates of the bifurcation points denoted by,

$$(\Psi^+, T^+), (\Psi^-, T^-). \tag{2}$$

In this context, $\Psi^{\pm}$ represents the normalized values of the AMOC intensity, where the system transitions from its nominal stable equilibrium state (Ψ^+) to its collapsed equilibrium state, and from the collapsed equilibrium state (Ψ^-) back to the nominal equilibrium state. The $T^{\pm}$ values denote the critical temperature anomaly forcing at which the two aforementioned bifurcations occur within the system. It should be noted that the method used to measure the AMOC strength may vary from one simulator to another. In this study using cGENIE, the definition chosen to quantify the maximum AMOC strength will be specified in the Results section. The Eq.(1) in the $EXPA$ experiment can be written as,

$$\frac{d\Psi}{dt} = \left(-\Psi^3 + a_1\Psi^2 + b_1\Psi + c_1 + d_1 T + e_{12}F^A_{GIS}\right)\frac{1}{\tau}, \tag{3}$$

where F^A_{GIS} represents the arbitrary constant value of the freshwater flux forcing applied during the first calibration experiment. Consequently, $c_1 + e_{12}F^A_{GIS}$ is a constant term in this experiment, effectively reducing the conceptual model to a single-forcing experiment. With this simplification enables we can calibrate the parameters within the technique proposed by Martinez Montero et al. (48) :

$$a_1 = \frac{3(\Psi^- + \Psi^+)}{2} \tag{4}$$

$$b_1 = -3\Psi^-\Psi^+ \tag{5}$$

$$c_1 = \frac{T^+\Psi^{-^2}(\Psi^- - 3\Psi^+) - T^-\Psi^{+^2}(\Psi^+ - 3\Psi^-)}{2(T^- - T^+)} - e_{12}F^A_{GIS} \tag{6}$$

$$d_1 = -\frac{(\Psi^+ - \Psi^-)^3}{2(T^+ - T^-)} \tag{7}$$

We define $EXPB$ as the second calibration experiment examining the AMOC intensity response to freshwater forcing, using the same simulator. The freshwater flux parameterization in the simulator is implemented as a hosing tipping experiment. From this experiment, we can extract the coordinates of the bifurcation points,

$$(\Psi^+, F^+_{GIS}), (\Psi^-, F^-_{GIS}). \tag{8}$$

$F^{\pm}_{GIS}$ represents the critical values of the freshwater flux forcing at which the bifurcation of the AMOC occurs. By defining T^B as the constant value of the temperature anomaly imposed during this second calibration experiment, Eq.(1) can be expressed as:

$$\frac{d\Psi}{dt} = (-\Psi^3 + a_1\Psi^2 + b_1\Psi + c_1 + d_1T^B + e_{12}F_{GIS})\frac{1}{\tau}. \quad (9)$$

Here, $c_1 + d_1T^B$ represents the constant term, and the method proposed by Martinez Monteiro et al. (48) enables the determination of two new values for the following parameters,

$$c_1 = \frac{F^+_{GIS}\Psi^{-^2}(\Psi^- - 3\Psi^+) - F^-_{GIS}\Psi^{+^2}(\Psi^+ - 3\Psi^-)}{2(F^-_{GIS} - F^+_{GIS})} - d_1T^B, \quad (10)$$

$$e_{12} = -\frac{(\Psi^+ - \Psi^-)^3}{2(F^+_{GIS} - F^-_{GIS})}, \quad (11)$$

Thus, from the five unknowns $(a_1, b_1, c_1, d_1, e_{12})$ and two forcing variables, independent calibration experiments allows us to apply the methodological framework of Martinez Monteiro et al. (48) to reduce to the case of a single forcing variable. This results in six equations with an over-determination of the independent parameter c_1. It is possible to generalize the approach to include more than two forcing variables. For instance, as demonstrated in the Supplementary Materials (S2), an additional freshwater flux forcing term was incorporated into Eq. (1), which can be used for instance to calibrate the impact of variations in glacier melt under future scenarios. Mathematically, the generalization to N forcing variables results in obtaining $4N - 2(N-1)$ equations with $4 + (N-1)$ knowns and $N-1$ over-determined equations. As shown in the next section, these over-determinations occur because the coefficient c_1 is the constant shared across all calibrations of different sensitivity experiments. What value, then, should be assigned to c_1? Sensitivity experiments have shown that defining $c_1 = c_1^A$, where c_1^A is determined from Eq.(6), yields the most accurate results for emulating the evolution of the AMOC based on the simulator. This is because temperature forcing is the primary driver of AMOC collapse (15), as demonstrated in CMIP5 experiments (13). Consequently, we prioritize achieving the most accurate calibration for temperature forcing while tolerating a greater error in calibrating freshwater forcing. Therefore, we adopt the value of c_1 as determined by the temperature sensitivity calibration experiment.

The final parameter in the ATCM module that needs to be calibrated is the internal dynamic time scale of the AMOC, denoted as τ. Based on Armstrong McKay et al. (50), we assume that the internal dynamic time scale of the AMOC is the same whether it is collapsing or recovering, i.e., $\tau \equiv \tau^+_\Psi = \tau^-_\Psi$. To calibrate τ, we aim to minimize the discrepancy between the timing of the AMOC collapse in the simulator and in the emulator. This is achieved through classical numerical optimization to determine the optimal τ calibration in the emulator, allowing a maximum tolerance of 1% difference between the projected timings in the two models.

What type of forcing experiment should be conducted with the simulator for this purpose? By definition, τ requires transient experiments measuring AMOC intensity in our simulator. As we show next, this simplified AMOC dynamics framework cannot simultaneously reproduce with equal accuracy the characteristic timescales of AMOC response to both rapid and slow forcing regimes. Hence, the user should chose a forcing function that is consistent with the emulator's intended application. Here, given our emulator's primary purpose of investigating plausible near-term AMOC collapse scenarios, we calibrate τ in the following section using a cGENIE simulation where atmospheric CO_2 concentrations increase by 1% annually until reaching eight times pre-industrial levels. We will subsequently demonstrate the robustness of these calibration results while discussing their inherent limitations.

3. Results

In this section, we calibrate the ATCM using cGENIE, following the methodology developed in Section 2. Next, we evaluate the ATCM by simulating the AMOC under two SSP scenarios and comparing the results with cGENIE simulations. Finally, we integrate the ATCM into SURFER and simulate the evolution of the AMOC under a range of realistic emission scenarios.

3.1 Calibration with cGENIE

To validate the emulator, we applied the ATCM to cGENIE (51), an EMIC (37) that has already demonstrated its ability to simulate AMOC hysteresis (14,52). cGENIE includes an ocean circulation model (3D), a dynamic-thermodynamic sea ice model (2D) and an atmospheric energy moisture balance model (2D). The ocean model accounts for the horizontal and vertical transport of heat, salinity and biogeochemical tracers. The circulation is simulated through advection, convection, and mixing (52,53). In cGENIE, the maximum AMOC strength is defined as the maximum value of the overturning stream function below approximately 1000 meters depth in the Atlantic. This depth threshold ensures that shallow convection associated with surface gyres is not included, even in cases where the AMOC has collapsed. cGENIE has a very simple atmospheric model, which results in a minimal effect of net changes in the Precipitation-Evaporation (P-E) balance over the North Atlantic due to global warming. However, if the ATCM is applied to emulate a simulator that account for variations in the P-E balance, these would be captured in the calibration through the temperature anomaly. cGENIE does not include an explicit parameterization of GIS melt. Although such a component is not strictly required in the simulator targeted for emulation, its absence in cGENIE simplifies the calibration process: during the temperature-forcing calibration, we can be confident that no freshwater flux from the GIS affects the AMOC. This, in turn, simplifies the analysis of the AMOC's sensitivity to a single forcing through temperature in cGENIE. Following the experimental framework outlined in the Methods section, we conducted two independent sensitivity experiments to calibrate the $(a_1, b_1, c_1, d_1, e_{12})$ parameters using cGENIE.

The first experiment, labelled $EXPA$, consist of a 20,000-year simulation with a prescribed CO_2 forcing designed to generate a global atmospheric mean temperature anomaly. We thus apply our operational hypothesis by forcing the AMOC in cGENIE solely through temperature in this initial setup. To do so, we do not apply any artificial, time-dependent freshwater input at this stage. Accordingly, we define $F_{GIS}^{A} = 0\ Sv$ as the constant and arbitrary freshwater forcing value in $EXPA$. The CO_2, hence temperature forcing is parameterized as a linear increase from 280 ppm to 2,800 ppm. Through the internal dynamics of cGENIE, this forcing is translated into a global mean surface air temperature anomaly, starting from $T = 0°C$ for the initial thousands of years and reaching $T = 10°C$ after 20,000 years (see Supplementary Figure S1). This setup enables us to cover the plausible range of the AMOC tipping point location in terms of temperature forcing (5,50) while ensuring near-equilibrium conditions for the AMOC.
The second independent calibration experiment, labelled $EXPB$, involves a 20,000-year hosing simulation with freshwater flux forcing linearly increasing from 0 Sv to 0.2 Sv (see Supplementary Figure S2). For the constant value of the global mean temperature anomaly in this experiment, we set $T^B = 0°C$. The freshwater forcing values are chosen to align with the plausible range of AMOC tipping point locations associated with freshwater perturbations (18,27) and to be sufficient to trigger an AMOC collapse in cGENIE. The total salinity of the oceans is maintained constant in the simulation by applying a compensatory freshwater flux over the Pacific. The freshwater hosing is applied between $20°N$ and $50°N$ across the full width of the Atlantic (see Figure S3) to reproduce the hosing region by Rahmstorf et al. (28). The durations of the $EXPA$ and $EXPB$ simulations are chosen to ensure that the AMOC is forced sufficiently slowly, allowing it to remain in near a stable state throughout the calibration experiments.

The two trajectories of the AMOC intensity obtained with cGENIE in the $EXPA$ and $EXPB$ experiments are shown in Figure 2. This three-dimensional representation, combining the two-dimensional forcing space with the additional AMOC intensity dimension, makes it possible to visualise the full range of possible forcing conditions for the AMOC, which the emulator will subsequently be able to explore. In the Supplementary Materials, Figures S4 and S5 show the bifurcation diagrams of the AMOC in the two-dimensional plane of the $EXPA$ and $EXPB$ experiments.

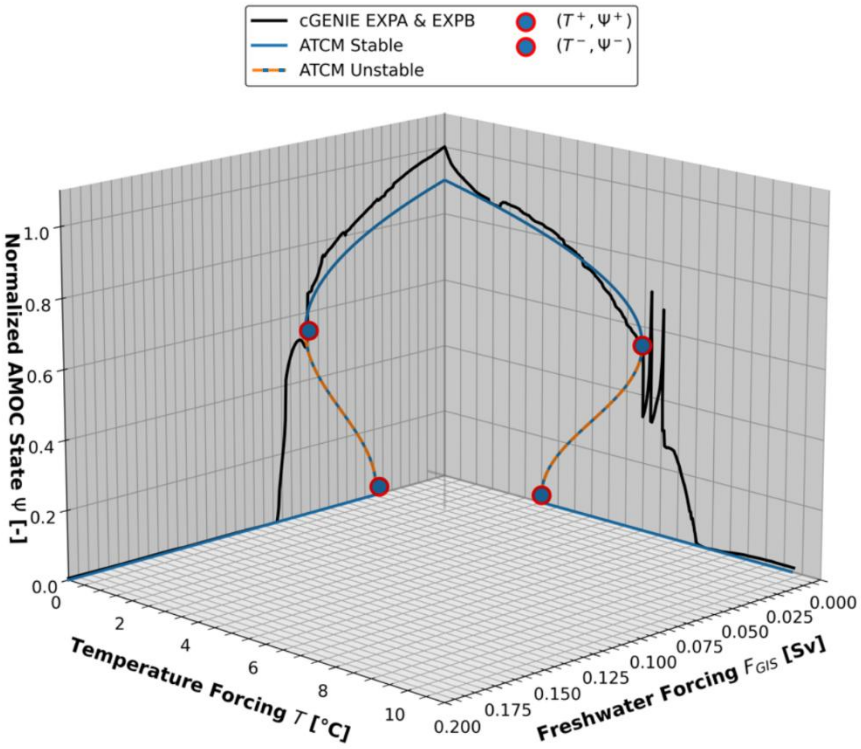

Figure 2 : Bifurcation diagrams of cGENIE and ATCM in the (T, F_{GIS}) forcing space. The two simulations produced by cGENIE during the calibration experiments $EXPA$ and $EXPB$ are shown in their respective planes as solid black lines. The identification of the bifurcation points based on these collapsed branches is marked in red, while the simplified hysteresis produced by the ATCM is shown in blue. The branch of the unstable equilibrium, which separates the two stable equilibria, is represented by the orange dashed line.

Since the primary objective of the ATCM is to accurately calibrate the collapse branch, we focus exclusively on simulating collapse scenarios with cGENIE. This allows to extend the duration of the simulations with the complex model and thus, obtain an AMOC as close as possible to its equilibrium in the simulator. In other words, a complete hysteresis cycle was not performed to refine our calibration of the collapse branch, but this does not undermine the validity of the results. As demonstrated in Laridon (54), the ATCM can also successfully emulate the AMOC trajectory of the simulator through the second bifurcation point. However, to achieve an optimal fit for the collapse trajectory, slight deviations from the bifurcation point coordinates provided by the simulator may enhance the emulator's accuracy in capturing the collapse dynamics. Accordingly, the values of $\Psi^- = 0.022, T^- = 3°C$ and $F_{GIS}^- = 0.037\ Sv$ were selected, as they minimise the calibration error along the trajectory of the nominal stable equilibrium. However, if the research objective is to accurately calibrate the recovery transition, it is possible to provide the emulator with the values of T^- and F_{GIS}^- corresponding to those identified in a full hysteresis experiment. A trade-off must therefore be made in the choice of the bifurcation point coordinates, in order to distribute the emulator's calibration error where it is most relevant with respect to the scientific objective.

All coordinates of the bifurcation points used in this study are given in Table 1. There is no standardised method for determining the precise location of bifurcation points. Consequently, the selection should be based on expert judgment and a comprehensive understanding of the simulator behaviour. In the ATCM model, Eq.(1) imposes that $\Psi_A^+ = \Psi_B^+ \equiv \Psi^+$ and $\Psi_A^- = \Psi_B^- \equiv \Psi^-$ to keep the number of unknows to a manageable level. Moreover, we aim to find the best fit for temperature forcing, so we define $\Psi^\pm \equiv \Psi_A^\pm$. Using these values, we compute the parameters $(a_1, b_1, c_1, d_1, e_{12})$, according to Eq. (4-7, 11), and the results are presented in Table 2. Based on the calibration of these parameters, the simplified hysteresis loop emulated by the ATCM is shown in Figure 2. Since we calibrated the ATCM using the c_1 value from $EXPA$, the double-fold structure passes precisely through the upper bifurcation point (T^+, Ψ^+) identified on the cGENIE curve from the temperature forcing calibration experiment. This is not the case for $EXPB$, as will be explained in the Discussion section. Indeed, there is a $0.002Sv$ difference between the F_{GIS}^+ tipping point identified from cGENIE and the value computed by the ATCM,

resulting in a relative difference between the two of 2.53%. Overall, the collapse dynamics demonstrate a reasonably good calibration against the cGENIE simulations.

	$\Psi^+ [Adim]$	$\Psi^- [Adim]$	$T^+ [°C]$	$T^- [°C]$	$F^+_{GIS} [Sv]$	$F^-_{GIS} [Sv]$	$F^A_{GIS} [Sv]$	$T^B [°C]$
EXPA	0.545	0.022	5.93	3	/	/	0	/
EXPB	0.545	0.022	/	/	0.075	0.037	/	0

Table 1 : Bifurcation coordinates. The values for Ψ^+, T^+, F^+_{GIS} are retrieved from the cGENIE calibration sensitivity experiments $EXPA$ and $EXPB$ shown in Figure 2. The Ψ^-, F^-_{GIS} and T^- values are manually fixed during the calibration procedure and adjusted to improve the fit of the collapse branch. The F^A_{GIS} and T^B values correspond to the arbitrary constant forcing applied during the sensitivity experiment.

a_1	b_1	c_1	d_1	e_{12}
0.851	-0.036	0.074	-0.024	-1.882

Table 2 : Internal dynamics parameter. The parameters are computed with the ATCM using Eq.(7-10,14) using coordinates of the bifurcation points given by Table 1.

Finally we must set τ, the characteristic timescale of AMOC dynamics. Following the experimental protocol outlined in the Methods section, we performed a third calibration experiment with cGENIE, labelled $EXPC$, spanning 1,250 years. The simulation was initialized at 280 ppm atmospheric CO_2 (pre-industrial level) and increased concentrations by 1% per year until reaching 2240 ppm (8× pre-industrial levels), maintaining this concentration thereafter (see Supplementary Figure 6). This calibration experiment applied only thermal forcing, without freshwater hosing. The cGENIE simulation reveals a minimum in the maximum AMOC intensity ($\Psi = 0.03$) by 2190 CE, followed by a partial recovery to less than 10% of its initial strength (Figure 3). This behaviour reflects residual, persistent deep convection below $1000m$ in our simulator, which gradually diminishes over longer time scales, as confirmed by additional analyses. We therefore define AMOC collapse in cGENIE as the event occurring by 2190 CE. We find that a value of $\tau = 18.94\ yr^{-1}$ best reproduces the the timing of this event in the emulator (Figure 3b).

While reproducing the timing of collapse, significant differences in the trajectories emerge between the emulator and the simulator outputs. This discrepancy stems primarily from: (i) the emulator's simplified single-equation framework, which lacks spatial resolution compared to cGENIE's 3D dynamical ocean physics, and (ii) the emulator's inability to capture rate-dependent AMOC modifications (R-tipping phenomena (32)) that are present in cGENIE. We further address these aspects in the validation experiments and discussion. Notably, the choice of $EXPC$ imposes operational constraints—if the emulator is intended for studying slower forcing regimes, alternative transient simulations would provide a more suitable calibration baseline (see Figure S7). The ATCM's minimal parameterization does not allow for universal calibration across all forcing timescales. However, as demonstrated in the following section, our 1% CO_2 forcing in EXPC enables robust emulator performance when applied to SSP scenarios, which constitute the primary focus of this study.

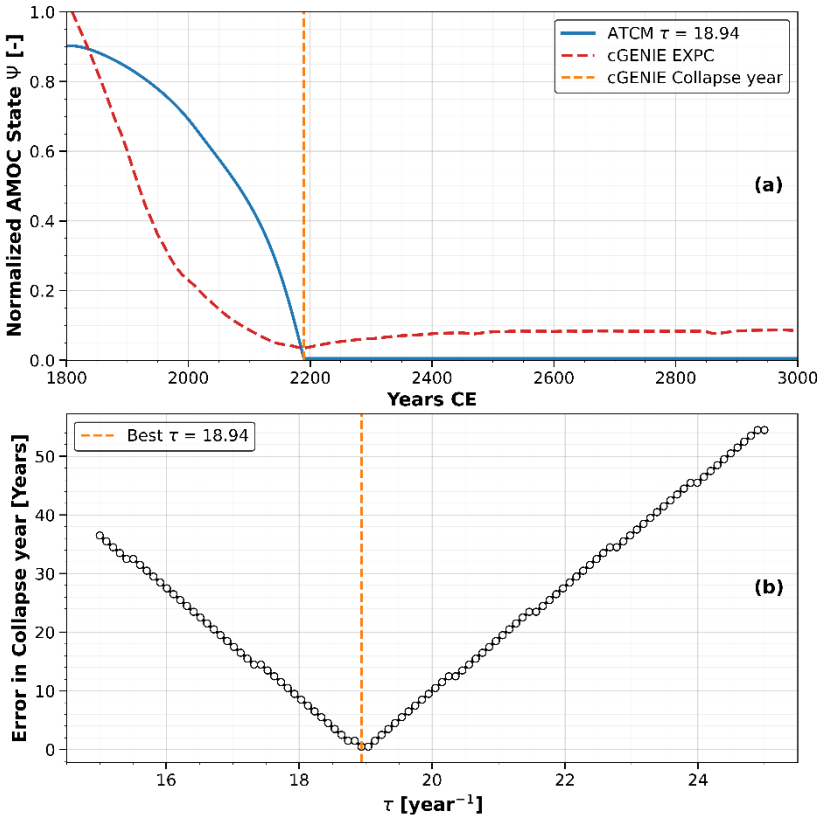

Figure 3: (a) Normalized AMOC intensity in the *EXPC* calibration experiment within the ATCM (blue) and cGENIE (red). **(b) ATCM Optimization of the τ parameter** to replicate the collapse year in cGENIE.

3.2 Validation of the emulator

To validate the emulator, we assess the ability of the ATCM to reproduce the AMOC trajectory simulated by cGENIE under four forcing combinations that differ from the ones used in the calibration experiments. Since the primary purpose of the emulator is to generate simulations for relatively near-term and realistic future scenarios, we selected two SSP simulations, namely SSP2-4.5 and SSP5-8.5. For each of these two SSP simulations, which prescribe distinct CO_2 concentration pathways and thus different temperature forcings, we additionally consider a configuration in which a constant hosing of $0.06\,Sv$ is applied in the same region as in previous cGENIE experiments. The resulting temperature anomalies in cGENIE are presented in Supplementary Figure S8. The four normalized AMOC trajectories from these validation experiments are shown in Figure 4 as solid lines. In cGENIE, the AMOC does not collapse under SSP2-4.5 without hosing, but does collapse under SSP5-8.5 without hosing. The most striking result is that the AMOC does collapse under SSP2-4.5 when freshwater forcing is applied. Under SSP5-8.5, the collapse is naturally faster when hosing is included than when it is not.

We now examine the trajectories produced by the ATCM, shown in Figure 4 as solid lines. First, we note that whenever the AMOC collapses in cGENIE, it also collapses in the emulator, and similarly, when the AMOC remains active in the simulator, it remains active in the emulator. This constitutes the minimal criterion for the emulator's skill—namely, the ability to correctly predict whether a collapse occurs in the simulator. Second, regarding the timing of the collapse, the emulator consistently predicts it to occur earlier than in cGENIE. This discrepancy is most pronounced for the SSP2-4.5 scenario with hosing, which represents the lowest forcing rate among the validation experiments. We recall that the parameter τ was calibrated using the $EXPC$, based on a transient experiment with a 1% increase in atmospheric CO_2 concentration per year. This forcing pathway has a rate of forcing closer to that of SSP5-8.5. This explains why the emulator performs particularly well for the SSP5-8.5 scenario without hosing, reproducing the timing of the complete collapse within only six years of cGENIE (2350 CE in cGENIE versus 2356 CE in the ATCM).

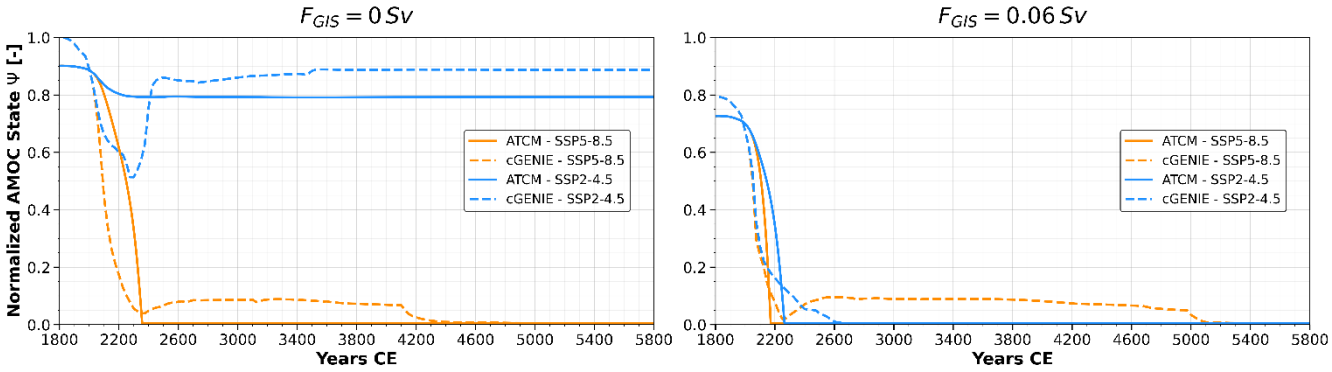

Figure 4. Trajectories of the AMOC in the validation experiments with the emulator and the simulator under SSP scenarios without additional hosing (left) and with additional hosing (right). Solid lines correspond to the ATCM, while dashed lines correspond to the simulator.

This said, even under SSP2-4.5, the ~350-years difference in the timing of total collapse between the two models is acceptable, especially considering that by 2240 CE both models predict an AMOC intensity below 15%, which already indicates an abrupt and nearly complete collapse. Third, the emulator successfully reproduces the AMOC collapse under SSP2-4.5 when hosing is applied. This achievement results from the novel representation of the AMOC in the ATCM, which incorporates an additional freshwater flux forcing variable calibrated against the target simulator. We see this as a significant result. Finally, the differences between the emulator and cGENIE trajectories arise from the spatial and physical dynamics represented in cGENIE but absent from the emulator. In particular, cGENIE captures the fact that the changes in AMOC intensity not only depends on the absolute magnitude of the forcings but also on their rate of change over time. This phenomenon, known as rate-induced tipping (R-tipping (32)), can lead to substantial discrepancies between the two models. For instance, under the SSP2-4.5 scenario without hosing, between 2000 CE and 2400 CE when the rate of warming is the highest, the emulator projects an AMOC strength nearly 30% higher than in cGENIE. Similarly, in the other simulations, the emulator systematically overestimates the AMOC strength during the collapse phase due to its inability to capture rate-induced tipping. In practice, calibrating τ using the $EXPC$ —which involves a relatively high forcing rate compared to the validation experiments—partly compensates for this limitation.

3.3 ATCM Integration within the SURFER Climate Model

We now incorporate the ATCM emulator into the reduced-complexity climate model SURFER (see Figure 5) to explore a wider forcing space under realistic future scenarios. SURFER features a process-based carbon cycle capable of reliably simulating atmospheric CO_2 concentrations and global mean temperature changes. This reduced-complexity model also simulates sea-level rise and various ocean acidification metrics in response to anthropogenic greenhouse gas emissions, while enabling simulations over timescales ranging from decades to millions of years (48,49). Version 3.0 of SURFER comprises 17 differential equations that describe carbon exchanges among six reservoirs: the atmosphere, terrestrial systems, upper, intermediate, and deep ocean layers, and deep-sea sediments (49). Additionally, it models temperature anomalies across ocean layers, ice sheet volumes for Greenland and Antarctica, and sea-level changes due to glacier dynamics. SURFER has proven effective for integrating tipping element dynamics into climate simulations, as demonstrated by Couplet et al. (40). At the time of this project, version 3.0 of SURFER was not yet available. Therefore, we chose to integrate the ATCM into a preliminary version of v3.0 (see Data Availability), which we refer to here as pre3.0. There are no major differences between pre3.0 and v3.0. Some changes in the parameterization of SURFER's carbon cycle remain, but they are not central to the objectives of this study. To integrate the ATCM into SURFER pre3.0, we chose to deactivate all components associated with tipping elements other than the AMOC and GIS in order to specifically isolate the contributions of the new AMOC representation.

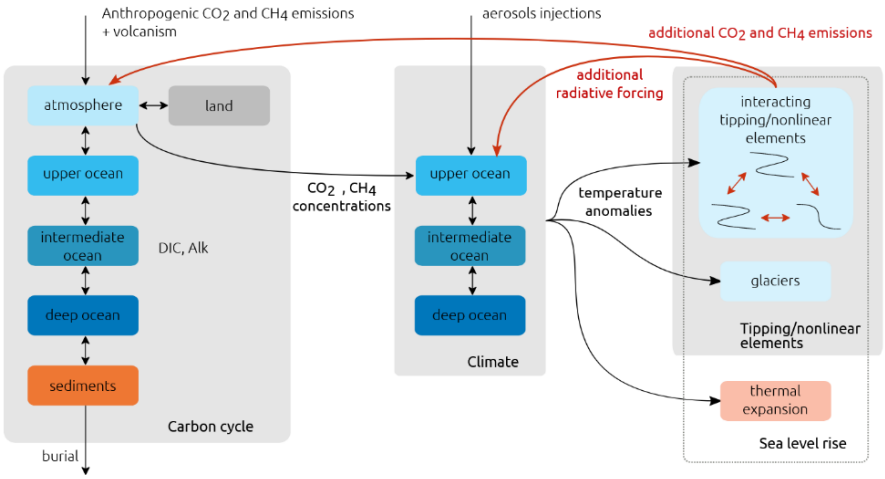

Figure 5 : Conceptual diagram of SURFER, including interacting tipping elements and their feedback on climate. Figure reproduced with permission from Couplet et al. (40). The ATCM is integrated into the 'Tipping Elements' box of SURFER.

Within SURFER we obtain dynamic projections of the mean atmospheric temperature anomaly T and the freshwater flux associated with GIS melting, all computed within a limited time. Indeed, the parameterisation of F_{GIS} follows that of Couplet et al. (40) and is defined as:

$$F_{GIS} = - \alpha_{GIS} \frac{dV}{dt}. \tag{12}$$

The freshwater contribution of the GIS is proportional to the temporal variation of its dimensionless volume V. As with the normalization of Ψ, the value of V is normalized by the volume of the GIS during the pre-industrial period. The parameter α_{GIS} relates the temporal variation of the dimensionless fraction of the GIS to a freshwater flux. The details of its computation and value are provided in Couplet et al. (40). In this pre-3.0 version of SURFER, we also use the same equation and calibration coefficients as in SURFER v2.0 (48) to describe the temporal evolution of the GIS volume,

$$\frac{dV}{dt} = \left(\overbrace{-V^3 + a_2 V^2 + b_2 V + c_2}^{internal\ dynamics} + \underbrace{d_2 T}_{forcing} \right) \mu_V(V). \tag{13}$$

The term $\mu_V(V)$ encodes the dynamic time scale of the GIS, analogous to that of the AMOC, except that this value is parameterized differently depending on whether the GIS is regaining ice volume ($\tau_V^+ = 5500\ yr^{-1}$) or melting it ($\tau_V^- = 470\ yr^{-1}$). These values are those used in SURFER v2.0 (47) and are themselves derived from a calibration against a complex GIS model. Note that it is possible to add in Eq.(13) a second forcing term proportional to (1 – Ψ) to account for the stabilising effect of a weakened AMOC on GIS melting. In Section S1 of the Supplementary Materials, we show how this two-forcing-variable equation can be calibrated, similarly to the ATCM. This tool can then be used to investigate tipping cascades (33,35) between these two systems with what we could call a tipping cascade emulator.

Figure 6 illustrates the fifteen emission scenarios selected as inputs to simulate the evolution of the AMOC within the emulator once integrated into SURFER. These emission trajectories follow the historical record from 1750 to 2010 CE, and are then extended using a logistic equation so that the cumulative emissions from 1750 to 2500 CE range from 1000 to 5000 PgC (55). In this way, they cover the spectrum from SSP1-2.6 to SSP5-8.5.

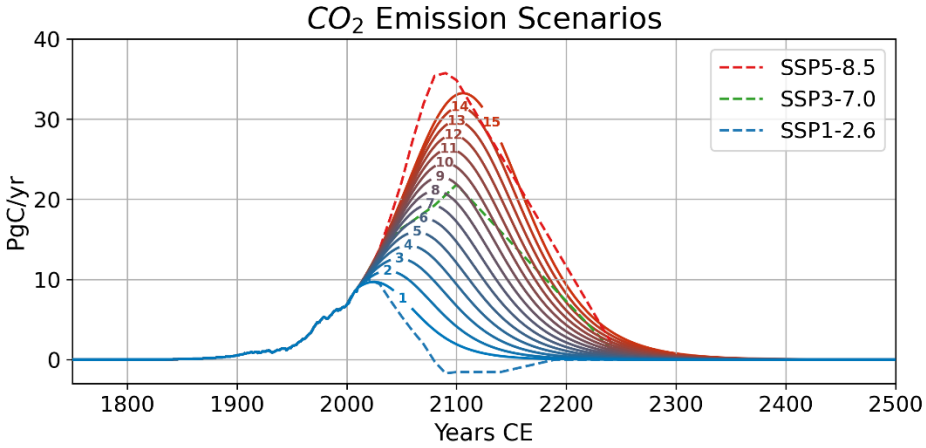

Figure 6 : Fifteen emission scenarios used as input to SURFER. These scenarios account for cumulative release of CO_2 in the atmosphere between 1000 to 5000 PgC since 1750 CE, and cover a similar range as the SSP scenarios. The emission trajectories range from blue for scenarios with the lowest emissions to red for those with the highest greenhouse gas emissions, with their corresponding labels placed directly along the curves.

3.4 Critical Manifold and Sampling the Forcing Space

Based on the calibration of the ATCM to cGENIE, we can represent in the forcing variable space (T, F_{GIS}), the two calibration experiments, $EXPA$ and $EXPB$, as well as the validation experiment that consider hosing (see Figure 7). This representation demonstrates the use of the emulator as a tool for mapping the forcing space of a given simulator. The critical manifold W_c is defined by the ATCM as follows,

$$W_c(T) = \frac{d_1}{e_{12}}(T^+ - T). \tag{14}$$

This manifold delineates the forcing space into two regions: one where the linear combinations of the variables T and F_{GIS} do not lead to an AMOC tipping in the emulator, and another where such combinations would, at equilibrium, drive the AMOC into the collapsed stable state. Despite the approximations inherent in the calibration process, the ATCM provides a valuable pre-diagnostic tool for analysing forcing combinations that, if sustained for a sufficient duration (32), are expected to lead to a complete tipping of the AMOC. For example, we can use this critical manifold to identify the tipping point according to the emulator for the SSP experiments with a $0.06\,Sv$ hosing applied in the specific region within cGENIE. In this way, the ATCM provides an estimate indicating that the tipping point associated with the temperature anomaly is near 1.2°C. This estimate is thus obtained through the emulator without the need to perform a new computationally expensive hysteresis experiment in cGENIE, which would combine both temperature and freshwater flux forcing.

As an application, we investigated the response of the ATCM integrated into SURFER under 15 emission scenarios, ranging from SSP1-2.6 to SSP5-8.5 (see Figure 6). Figure 8 shows the trajectories of these 10,000-year simulations in the forcing space (T, F_{GIS}). The critical manifold W_c is of course identical to that in Figure 7, derived from the ATCM through the calibration experiments $EXPA$ and $EXPB$. Nine of the 15 trajectories (labelled 7–15 in Figure 6) exceed the bifurcation threshold of the AMOC when considering the linear combination of the two forcing variables; in other words these trajectories cross W_c. Notably, trajectory 7 surpasses this threshold only briefly and weakly, resulting in the overshoot-without-tipping behavior described by Ritchie et al. (31). Hysteresis effects are evident: trajectories 8–14 lead to AMOC collapse and do not recover circulation despite returning to the safe space. Lastly, these results underscore the importance of accounting for both temperature and freshwater flux, as the inclusion of freshwater forcing lowers the temperature-associated tipping point due to their combined influence, as reflected in the slope of W_c.

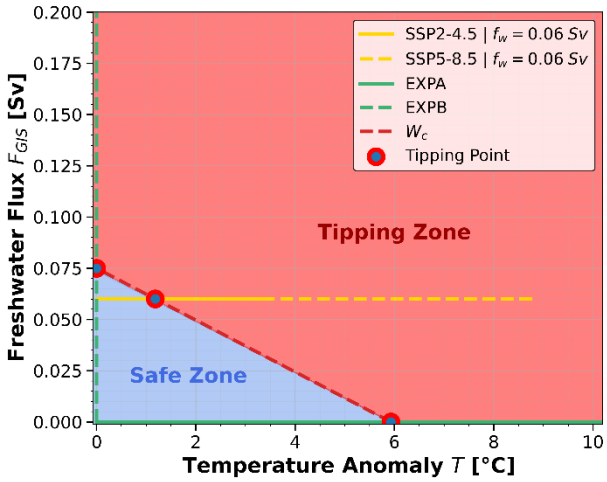

Figure 7 : Forcing space (T, F_{GIS}) showing calibration experiments *EXPA* (solid green line) and *EXPB* (dashed green line), along with two SSP validation experiments under hosing conditions (solide yellow line for SSP5-8.5 and dashed yellow line for SSP2-4.5). The tipping points identified in *EXPA* and *EXPB* are indicated by the blue and red markers. The red dashed line, W_c, represents the critical bifurcation manifold in the ATCM. The "Safe Zone" in the forcing space corresponds to the combinations of the two forcing variables that do not reach the bifurcation point, whereas the "Tipping Zone" corresponds to conditions exceeding this bifurcation threshold in the ATCM.

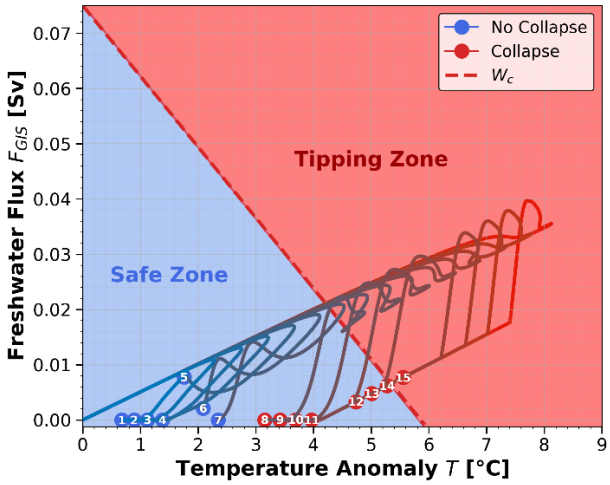

Figure 8: Evolution of Temperature (T) and Greenland meltwater flux (F_{GIS}) in SURFER under 15 emission scenarios (see Figure 6). The dots indicate the state of the AMOC at the end of the 10,000-year simulation: a blue dot represents $\Psi > \Psi^+$, corresponding to an active AMOC state, while a red dot represents $\Psi < 0.1$, indicating a collapsed state. The labels corresponding to their associated emission scenarios (see Figure 6) are written in white inside these dots. The red dashed line, W_c, denotes the critical bifurcation manifold in the ATCM, dividing the forcing space into the same two regions as defined in Figure 7.

3.5 New Collapse Trajectories Captured by the Emulator

To highlight the importance of developing an AMOC emulator that accounts for both temperature and freshwater flux forcing within a reduced-complexity climate model, we compared two cases using the ATCM in SURFER. In the first case, both forcings are included; in the second, the freshwater flux forcing is deliberately disabled. In both cases, we applied the emission scenarios shown in Figure 6. When the freshwater flux forcing from GIS melting is deactivated (see Figure 9a), only the five highest emission scenarios (labelled 11 to 15) lead to an AMOC collapse during these 10,000-year simulations. However, when the freshwater forcing from the GIS is activated in SURFER, three additional scenarios (labelled 8 to 10) result in an AMOC collapse. These three scenarios correspond to total cumulative emissions ranging from 3000 PgC to 3571 PgC over the period 1750–2500 CE. In other words, they lie slightly below and above the cumulative total emissions associated with SSP3-7.0, as shown in Figure 6. Thus, in addition to reproducing the key result identified in the validation experiments—namely, that the emulator can simulate collapses that would not occur under temperature-only forcing—the emulator coupled with SURFER now allows the simulation of these collapse trajectories at low computational cost, without the need to rerun the full complex model.

Lastly, in these comparisons of the trajectories with the temperature bifurcation diagram computed by the emulator, two additional noteworthy observations can be made. When the freshwater flux forcing is excluded (see Figure 9a), the AMOC trajectories lie above the bifurcation diagram. In other words, the system is unable to track its stable equilibrium position. Indeed, rate of forcing changes shifts the AMOC significantly off the equilibrium position that would be observed in a hysteresis experiment. In Figure 9b, by contrast, the trajectories consistently lie below the temperature bifurcation diagram. This occurs because the trajectories are driven by two forcings, whereas here we are representing only the temperature bifurcation diagram (for the purpose of comparing the trajectories between Figures 9a and 9b) and not the bifurcation diagram corresponding to the combined effect of both forcings.

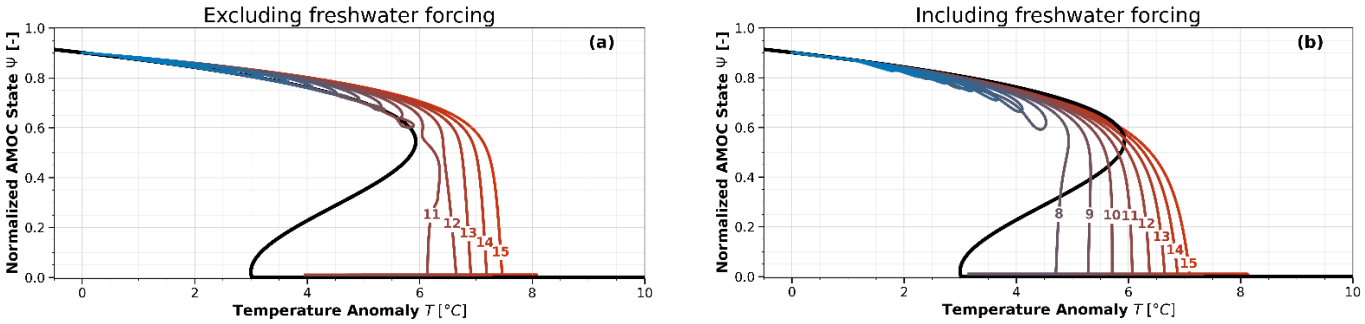

Figure 9: Temperature bifurcation diagram from the ATCM showing the 15 AMOC trajectories in the case where only temperature forcing is applied (a) and when freshwater forcing is also included (b). The 15 trajectories are computed based on the emissions scenarios described in Figure 6. AMOC trajectories are colored from blue for the lowest-emission scenarios to red for the highest-emission scenarios, with labels corresponding to those in Figure 6. The black curve represents the temperature bifurcation diagram computed by the ATCM based on $EXPA$.

4. Discussion

We developed a two-forcing-variable AMOC emulator that can be calibrated using only three calibration experiments. The differences between the ATCM and cGENIE during the calibration phase can be attributed to two factors: the inherent limitations of the conceptual approach and constraints within the ATCM calibration module. The first factor stems from the intrinsic simplifications involved in fitting a double-fold structure to a complex hysteresis. These limitations were expected. From a technical standpoint, fitting a third-order polynomial to a complex curve is expected to introduce a non-negligible discrepancy between the approximation and the behaviour of the full complex model. The challenge, therefore, is to identify the most effective approach to minimize this inherent error. In the following, we describe the origin of these approximations and the strategies implemented to mitigate their impact.

The first source of error in the calibration module arises from the values of the independent term c_1, which must take the same value across all sensitivity experiments. As outlined in the Methods section, the coefficient is over-determined across the two sensitivity experiments. Consequently, a specific value of c_1 is selected based on one calibration experiment, but this value may not apply to the other. This approach implies that our simplified model is calibrated to the bifurcation points of one calibration experiment (temperature forcing) but not the other (freshwater flux forcing). However, the decision to minimize error for temperature forcing is justified because this forcing is the dominant factor influencing the AMOC (13,14,56).
A second limitation of the ATCM is that we did not impose the value of the AMOC intensity at preindustrial levels, as doing so would introduce an additional constraint and thereby limit experimental flexibility.
Furthermore, in the calibration experiments $EXPA$ and $EXPB$, we used the following values for the forcings held constant: $F_{GIS}^{A} = 0\ Sv$ and $T^{B} = 0\ °C$. In principle, these parameters could be constant and not zero. However, there is a scientific rationale behind our choice. First, the prevailing approach in the literature when conducting AMOC hysteresis experiments is to vary one forcing while keeping the other (if included) fixed at zero. This helps reduce the spin-up period in the complex model simulations. Our methodological choice is therefore supported by a broader availability of simulation data. Finally, as shown in Figures 7 and 8, the emulator allows us to estimate the critical manifold of the emulated simulator by assuming that this manifold is a straight line. Given a similar uncertainty in the estimated position of each tipping point, the probability of accurately approximating the true line increases when the two bifurcation points used to define it are farther apart. However, if users wish to characterize the critical manifold in more detail, it would be valuable to conduct additional hysteresis experiments using non-zero constant values for F_{GIS}^{A} or T^{B}. This would make it possible to test the robustness of the assumption that the critical manifold is linear in the simulator.

In addition to the differences observed in fitting the bifurcation diagram, limitations of the emulator became apparent during the calibration of the τ parameter. Although we developed a method to numerically calibrate this parameter based on the identification of the collapse timing in the simulator,

Figure 3(a) reveals substantial differences between the two transient trajectories. This discrepancy arises because, in a complex model such as cGENIE, the AMOC may be sensitive not only to the absolute magnitude of the forcing but also to its rate of change over time. This rate dependence causes cGENIE to simulate a much more abrupt AMOC collapse than the ATCM, despite τ being calibrated so that the timing of the collapse matches in both models.

After calibrating the simplified AMOC dynamics, the emulator was tested in four additional experiments, including two that combined both forcing variables. The results indicate that the emulator performs well according to three criteria: (i) correctly predicting whether a collapse occurs in the simulator, (ii) reproducing the timing of such a collapse, and (iii) capturing the AMOC response under the combined influence of temperature and freshwater flux. For criteria (i) and (iii), the emulator reproduces the results of the simulator exactly. Regarding criterion (ii), the emulator tends to slightly anticipate the timing of a complete AMOC collapse compared to the simulator. This occurs in scenarios with weaker forcing than in our chosen $EXPC$ experiment, which applies a 1% per year increase in CO_2 concentration. Nevertheless, the AMOC intensity in the simulator is below 15% at that time, which can still be considered qualitatively as a collapsed state. These results demonstrate the emulator's capability to provide an accurate representation of near-future AMOC collapse trajectories under realistic emission scenarios. For studies involving much slower forcing rates, it would be advisable to use a transient AMOC experiment with a slower forcing than the 1% CO_2 increase per year $EXPC$. Otherwise, the emulator may overestimate even more the timing of total collapse (see Supplementary Figure S7).

Therefore, we argue that the resulting emulator is relevant. The calibration achieved provides a tool that closely approximates the behaviour of the simulator it emulates, making it suitable for practical use as an emulator. However, simulators, whether EMICs or even ESMs, still carry significant uncertainty regarding the exact location of the AMOC tipping points and, consequently, the timing of their collapse (5,50,56). In this context, the ATCM should not be regarded as a tool for delivering accurate projections. While it is highly likely that the emulator's values deviate from the process-based results of the simulator, we demonstrate that the emulator can be calibrated sufficiently well to provide plausible and relevant outcomes. This is a key requirement for an AMOC tipping element emulator, as it enables more accurate studies of the AMOC state under plausible future positions within its forcing space. As shown in the Results section (see Figure 7 and 8), the ATCM facilitates realistic sampling of the forcing space once integrated into a reduced-complexity climate model like SURFER. Where complex models face significant computational constraints, the presented emulator enables performing a large number of simulations at very low cost, while maintaining consistency with more complex models. These computationally-efficient simulations also allow for the study of overshoot without tipping scenarios (32) by sampling the bivariate forcing space with higher resolution (Figure 8).

A promising direction for future research is to calibrate the ATCM using an ensemble of EMICs and potentially ESMs, allowing exploration of both the forcing space and the critical thresholds of the models, while also accounting for model uncertainty. Furthermore, the calibration approach presented here can be generalized to incorporate additional forcing variables (see Supplementary Materials S2). Another promising avenue is the application of the ATCM methodology to the GIS (see Supplementary Materials), yielding a non-linear dynamics tool calibrated on simulators to investigate potential cascading collapses between the AMOC and GIS (33,35). Beyond the GIS, this framework for constructing tipping element emulators can be extended to other tipping elements, starting with the six additional elements whose initial parameterizations are included in an extended version of SURFER v3.0 (40). Finally, this emulator could be integrated into other reduced-complexity climate models, such as FAIR (57), with minimal technical adjustments, as it requires only the global mean temperature anomaly and a parameterization of the GIS freshwater flux as input from the climate model.

5. Conclusion

We have presented the AMOC Tipping Calibration Module (ATCM), an emulator of AMOC dynamics based on a double-fold bifurcation structure. For the first time, this emulator incorporates two forcing variables that can be calibrated using only three experiments from the target complex model, also called

the "simulator". The emulator reproduces the AMOC behaviour observed in these experiments, although simplified dynamics introduce differences during the transient phase. For example, simulators such as cGENIE capture rate-induced effects, which can only be partially compensated by calibrating the time scale parameter. Despite these limitations, the ATCM reliably: (i) predicts whether a collapse occurs, (ii) reproduces its timing, and (iii) captures the AMOC response under combined temperature and freshwater forcing. Across four validation experiments, the emulator correctly reproduces the occurrence of a collapse. The emulator systematically predicts the collapse slightly earlier than the simulator under forcing scenarios with slower rates than in the calibration experiment. Most notably, the emulator consistently reproduces AMOC collapse trajectories under simultaneous temperature and freshwater forcing.

In addition to reproducing AMOC behaviour according to these three criteria, the ATCM offers substantial computational advantages over complex models. When integrated into the reduced-complexity model SURFER, it enables efficient exploration of the forcing space across a range of emission scenarios. We demonstrated that three emission trajectories between SSP3-7.0 and SSP5-8.5 trigger an AMOC collapse in SURFER when the two-forcing emulator is included. Furthermore, the emulator enables the assessment of the linear complex model's critical manifold in the forcing space, specifying the combinations of temperature and freshwater forcing that result in a collapse at equilibrium. This allows systematic investigation of boundary cases and comparative sensitivity analysis.

Finally, the calibration methodology can be extended to other tipping elements. A next step would be to calibrate a Greenland Ice Sheet (GIS) emulator in a similar manner, enabling the study of potential cascading collapses between the AMOC and GIS at low computational cost. The emulator could also be implemented in other reduced-complexity models with minimal adjustment. Overall, we have established a robust framework for calibrating two-forcing tipping element dynamics, bridging conceptual and complex models. This tool can therefore enhance understanding of tipping element collapse trajectories, which remain poorly understood despite their profound societal implications.

Data availability

Laridon, A et al. Connecting complex and simplified models of tipping elements: a nonlinear two-forcing emulator for the Atlantic meridional overturning circulation. Zenodo. DOI : https://doi.org/10.5281/zenodo.14944240; 2025. This repository contains the data as well as the scripts, the SURFER model and the ATCM used in this study. The *ATCM.ipynb* Jupyter Notebook contains the Python code where the ATCM is defined, calibrated, and validated using cGENIE simulations. The *SURFER_pre3.0_ATCM.ipynb* Jupyter Notebook contains the integration of the ATCM into the SURFER pre3.0 climate model. These two notebooks were used to generate all the figures presented in this paper. The emission scenario data required to run the simulations implemented in SURFER can be found in the *data/SURFER/* directory within the Zenodo repository. More details on the definition of the emission scenarios used can be found in Appendix A.2 of V. Couplet's PhD thesis (55). The repository is available under Creative Commons Zero v1.0 Universal.
Laridon A et al. Supplementary Materials. Connecting complex and simplified models of tipping elements: a nonlinear two-forcing emulator for the Atlantic meridional overturning circulation. Zenodo. DOI : https://doi.org/10.5281/zenodo.14979157; 2025. This repository contains the supplementary materials referred in this paper (i) GIS calibration (ii) parameterization of the AMOC with three forcing variables (iii) supplementary Figures. The repository is available under Creative Commons Zero v1.0 Universal.
The code for the version of the 'muffin' release of the cGENIE Earth system model used in this paper, is tagged as v0.9.61, and is assigned a DOI: https://doi.org/10.5281/zenodo.15021902. Configuration files for the specific experiments presented in the paper can be found in the directory: genie-userconfigs/PUBS/published/Laridon_et_al_2025. Details of the experiments, plus the command line needed to run each one, are given in the readme.txt file in that directory. All other configuration files and boundary conditions are provided as part of the code release. A manual detailing code installation,

basic model configuration, tutorials covering various aspects of model configuration, experimental design, and output, plus the processing of results, is assigned a DOI: https://doi.org/10.5281/zenodo.13377225.

Author Contributions

AL, VC, and MC conceptualized the study and its objectives, which are based on AL's MSc thesis. AL and VC are responsible for the design of the ATCM methodology. AL conducted the formal and technical analysis of the project. MC and WT managed and coordinated the research activity planning and execution. MC, as the supervisor of AL's MSc thesis and co-supervisor of AL's PhD, and WT, as the supervisor of AL's PhD, provided oversight and guidance. JG assisted in designing the calibration experiments with cGENIE and conducted them. AL analysed, with the help of JG these simulations. AL integrated the cGENIE simulations into the ATCM. AL is responsible for the study's visualization, creation, and presentation of the published work. AL wrote the original draft, produced all the figures and led the manuscript writing process. AL, MC, JG, VC and WT reviewed and revised it.

Competing interests

No competing interests were disclosed.

Grant information

The majority of the technical work in this paper originates from the MSc Thesis of AL, completed in 2024 at UCLouvain (54) under the guidance of MC. The writing and finalization of the research for this article were conducted at the beginning of AL's PhD thesis under the guidance of WT at VUB. The PhD is funded by the FWO under File Number: 1151225N. This project has received funding from the European Union's Horizon 2020 research and innovation programme under grant agreement No 820970 (project TiPES). This project has also received funding from the European Research Council (ERC) under the European Union's Horizon 2020 research and innovation programme under grant agreement No 101081369 (project SPARCCLE).

Ethics and Consent

In accordance with the F1000 AI Policy, the authors confirm that they have used *ChatGPT (GPT-4, OpenAI, 2025)* during the preparation of this manuscript. The tool was employed exclusively for language editing purposes, specifically to improve the clarity, grammar, and academic tone of English translations. No content generation, conceptual development, or substantive modifications were delegated to the tool. All scientific content, interpretations, and conclusions remain entirely the work of the authors.

No additional ethical approval or consent was required.

References

1. Stocker TF. Chapter 1 - The Ocean as a Component of the Climate System. In: Siedler G, Griffies SM, Gould J, Church JA, editors. International Geophysics [Internet]. Academic Press; 2013 [cited 2024 Dec 10]. p. 3–30. (Ocean Circulation and Climate; vol. 103). Available from: https://www.sciencedirect.com/science/article/pii/B9780123918512000015

2. Jackson LC, Kahana R, Graham T, Ringer MA, Woollings T, Mecking JV, et al. Global and European climate impacts of a slowdown of the AMOC in a high resolution GCM. Clim Dyn. 2015 Dec 1;45(11):3299–316.

3. Liu W, Fedorov AV, Xie SP, Hu S. Climate impacts of a weakened Atlantic Meridional Overturning Circulation in a warming climate. Sci Adv. 2020 June 26;6(26):eaaz4876.

4. Lenton T, Held H, Kriegler E, Hall JW, Lucht W, Rahmstorf S, et al. Tipping elements in the Earth's climate system. Proc Natl Acad Sci. 2008 Feb 12;105(6):1786–93.

5. Lenton T, Laybourn L, Armstrong McKay D, Loriani S, Abrams JF, Lade SJ, et al. Global Tipping Point Report 2023 [Internet]. UK: University of Exeter; 2023. Available from: https://report-2023.global-tipping-points.org/

6. Van Westen RM, Kliphuis M, Dijkstra HA. Physics-based early warning signal shows that AMOC is on tipping course. Sci Adv. 2024 Feb 9;10(6):eadk1189.

7. Zickfeld K, Eby M, Weaver AJ. Carbon-cycle feedbacks of changes in the Atlantic meridional overturning circulation under future atmospheric CO2. Glob Biogeochem Cycles [Internet]. 2008 [cited 2024 Apr 4];22(3). Available from: https://onlinelibrary.wiley.com/doi/abs/10.1029/2007GB003118

8. Brovkin V, Brook E, Williams JW, Bathiany S, Lenton TM, Barton M, et al. Past abrupt changes, tipping points and cascading impacts in the Earth system. Nat Geosci. 2021 Aug;14(8):550–8.

9. Rocha JC, Peterson G, Bodin Ö, Levin S. Cascading regime shifts within and across scales. Science. 2018 Dec 21;362(6421):1379–83.

10. Buckley MW, Marshall J. Observations, inferences, and mechanisms of the Atlantic Meridional Overturning Circulation: A review. Rev Geophys. 2016;54(1):5–63.

11. Goosse H. Climate System Dynamics and Modelling: [Internet]. 1st edn. Cambridge University Press; 2015 [cited 2024 Apr 20]. Available from: https://www.cambridge.org/highereducation/books/climate-system-dynamics-and-modelling/C8FC9D02159C8D9FD2146976AA8D28A6#contents

12. Stocker TF, Schmittner A. Influence of CO2 emission rates on the stability of the thermohaline circulation. Nature. 1997 Aug;388(6645):862–5.

13. Levang SJ, Schmitt RW. What Causes the AMOC to Weaken in CMIP5? J Clim. 2020 Feb 15;33(4):1535–45.

14. Gérard J, Crucifix M. Diagnosing the causes of AMOC slowdown in a coupled model: a cautionary tale. Earth Syst Dyn. 2024 Mar 22;15(2):293–306.

15. Bakker P, Schmittner A, Lenaerts JTM, Abe-Ouchi A, Bi D, van den Broeke MR, et al. Fate of the Atlantic Meridional Overturning Circulation: Strong decline under continued warming and Greenland melting. Geophys Res Lett. 2016;43(23):12,252-12,260.

16. Bakker P, Schmittner A, Lenaerts JTM, Abe-Ouchi A, Bi D, van den Broeke MR, et al. Fate of the Atlantic Meridional Overturning Circulation: Strong decline under continued warming and Greenland melting. Geophys Res Lett. 2016;43(23):12,252-12,260.

17. Böning CW, Behrens E, Biastoch A, Getzlaff K, Bamber JL. Emerging impact of Greenland meltwater on deepwater formation in the North Atlantic Ocean. Nat Geosci. 2016 July;9(7):523–7.

18. Jackson LC, Alastrué de Asenjo E, Bellomo K, Danabasoglu G, Haak H, Hu A, et al. Understanding AMOC stability: the North Atlantic Hosing Model Intercomparison Project. Geosci Model Dev. 2023 Apr 6;16(7):1975–95.

19. Romanou A, Rind D, Jonas J, Miller R, Kelley M, Russell G, et al. Stochastic Bifurcation of the North

Atlantic Circulation under a Midrange Future Climate Scenario with the NASA-GISS ModelE. J Clim. 2023 Aug 21;36(18):6141–61.

20. Stommel H. Thermohaline Convection with Two Stable Regimes of Flow. Tellus. 1961;13(2):224–30.

21. Wang S, Foster A, Lenz EA, Kessler JD, Stroeve JC, Anderson LO, et al. Mechanisms and Impacts of Earth System Tipping Elements. Rev Geophys. 2023;61(1):e2021RG000757.

22. Jackson LC, Wood RA. Hysteresis and Resilience of the AMOC in an Eddy-Permitting GCM. Geophys Res Lett. 2018;45(16):8547–56.

23. Rahmstorf S, Box JE, Feulner G, Mann ME, Robinson A, Rutherford S, et al. Exceptional twentieth-century slowdown in Atlantic Ocean overturning circulation. Nat Clim Change. 2015 May;5(5):475–80.

24. Caesar L, Rahmstorf S, Robinson A, Feulner G, Saba V. Observed fingerprint of a weakening Atlantic Ocean overturning circulation. Nature. 2018 Apr;556(7700):191–6.

25. Jackson LC, Biastoch A, Buckley MW, Desbruyères DG, Frajka-Williams E, Moat B, et al. The evolution of the North Atlantic Meridional Overturning Circulation since 1980. Nat Rev Earth Environ. 2022 Apr;3(4):241–54.

26. Clement AC, Peterson LC. Mechanisms of abrupt climate change of the last glacial period. Rev Geophys [Internet]. 2008 [cited 2024 Dec 9];46(4). Available from: https://onlinelibrary.wiley.com/doi/abs/10.1029/2006RG000204

27. Rahmstorf S. Ocean circulation and climate during the past 120,000 years. Nature. 2002 Sept;419(6903):207–14.

28. Rahmstorf S, Crucifix M, Ganopolski A, Goosse H, Kamenkovich I, Knutti R, et al. Thermohaline circulation hysteresis: A model intercomparison. Geophys Res Lett [Internet]. 2005 [cited 2023 Oct 22];32(23). Available from: https://onlinelibrary.wiley.com/doi/abs/10.1029/2005GL023655

29. Weijer W, Cheng W, Drijfhout SS, Fedorov AV, Hu A, Jackson LC, et al. Stability of the Atlantic Meridional Overturning Circulation: A Review and Synthesis. J Geophys Res Oceans. 2019;124(8):5336–75.

30. Armstrong McKay DI, Staal A, Abrams JF, Winkelmann R, Sakschewski B, Loriani S, et al. Exceeding 1.5°C global warming could trigger multiple climate tipping points. Science. 2022 Sept 9;377(6611):eabn7950.

31. Ditlevsen P, Ditlevsen S. Warning of a forthcoming collapse of the Atlantic meridional overturning circulation. Nat Commun. 2023 July 25;14(1):4254.

32. Ritchie P, Karabacak Ö, Sieber J. Inverse-square law between time and amplitude for crossing tipping thresholds. Proc R Soc Math Phys Eng Sci. 2019 Feb 27;475(2222):20180504.

33. Klose AK, Donges JF, Feudel U, Winkelmann R. Rate-induced tipping cascades arising from interactions between the Greenland Ice Sheet and the Atlantic Meridional Overturning Circulation. Earth Syst Dyn. 2024 May 27;15(3):635–52.

34. Klose AK, Wunderling N, Winkelmann R, Donges JF. What do we mean, 'tipping cascade'? Environ Res Lett. 2021 Dec;16(12):125011.

35. Sinet S, von der Heydt AS, Dijkstra HA. AMOC Stabilization Under the Interaction With Tipping Polar Ice Sheets. Geophys Res Lett. 2023;50(2):e2022GL100305.

36. Wood RA, Rodríguez JM, Smith RS, Jackson LC, Hawkins E. Observable, low-order dynamical controls on thresholds of the Atlantic meridional overturning circulation. Clim Dyn. 2019 Dec 1;53(11):6815–34.

37. Claussen M, Mysak L, Weaver A, Crucifix M, Fichefet T, Loutre MF, et al. Earth system models of intermediate complexity: closing the gap in the spectrum of climate system models. Clim Dyn. 2002 Mar 1;18(7):579–86.

38. Liu W, Xie SP, Liu Z, Zhu J. Overlooked possibility of a collapsed Atlantic Meridional Overturning Circulation in warming climate. Sci Adv. 2017 Jan 4;3(1):e1601666.

39. Mecking JV, Drijfhout SS, Jackson LC, Andrews MB. The effect of model bias on Atlantic freshwater transport and implications for AMOC bi-stability. Tellus Dyn Meteorol Oceanogr [Internet]. 2017 Jan 1 [cited 2025 Jan 14];69(1). Available from: https://a.tellusjournals.se/articles/10.1080/16000870.2017.1299910

40. Couplet V and Crucifix M. Tipping interactions and cascades on multimillennial time scales in a model of reduced complexity. Submitted to Earth System Dynamics, 2025.

41. Dekker MM, von der Heydt AS, Dijkstra HA. Cascading transitions in the climate system. Earth Syst Dyn. 2018 Nov 6;9(4):1243–60.

42. Wunderling N, Donges JF, Kurths J, Winkelmann R. Interacting tipping elements increase risk of climate domino effects under global warming. Earth Syst Dyn. 2021 June 3;12(2):601–19.

43. Klose AK, Karle V, Winkelmann R, Donges JF. Emergence of cascading dynamics in interacting tipping elements of ecology and climate. R Soc Open Sci. 2020 June 24;7(6):200599.

44. Liu W, Liu Z. A Diagnostic Indicator of the Stability of the Atlantic Meridional Overturning Circulation in CCSM3. J Clim. 2013 Mar 15;26(6):1926–38.

45. Rahmstorf S. On the freshwater forcing and transport of the Atlantic thermohaline circulation. Clim Dyn. 1996 Nov 1;12(12):799–811.

46. de Vries P, Weber SL. The Atlantic freshwater budget as a diagnostic for the existence of a stable shut down of the meridional overturning circulation. Geophys Res Lett [Internet]. 2005 [cited 2024 Dec 10];32(9). Available from: https://onlinelibrary.wiley.com/doi/abs/10.1029/2004GL021450

47. Oakley JE, Youngman BD. Calibration of Complex Computer Simulators using Likelihood Emulation [Internet]. arXiv; 2014 [cited 2025 Oct 15]. Available from: http://arxiv.org/abs/1403.5196

48. Martínez Montero M, Crucifix M, Couplet V, Brede N, Botta N. SURFER v2.0: a flexible and simple model linking anthropogenic CO_2 emissions and solar radiation modification to ocean acidification and sea level rise. Geosci Model Dev. 2022 Nov 9;15(21):8059–84.

49. Couplet V, Martínez Montero M, Crucifix M. SURFER v3.0: a fast model with ice sheet tipping points and carbon cycle feedbacks for short and long-term climate scenarios. EGUsphere. 2024 Sept 11;1–77.

50. Armstrong McKay DI, Staal A, Abrams JF, Winkelmann R, Sakschewski B, Loriani S, et al. Exceeding 1.5°C global warming could trigger multiple climate tipping points. Science. 2022 Sept 9;377(6611):eabn7950.

51. Ridgwell A. cGENIE.muffin EMIC Documentation. 2022; Available from: https://www.seao2.info/mymuffin.html

52. Marsh R, Sóbester A, Hart EE, Oliver KIC, Edwards NR, Cox SJ. An optimally tuned ensemble of the

'eb_go_gs' configuration of GENIE: parameter sensitivity and bifurcations in the Atlantic overturning circulation. Geosci Model Dev. 2013 Oct 21;6(5):1729–44.

53. Edwards NR, Marsh R. Uncertainties due to transport-parameter sensitivity in an efficient 3-D ocean-climate model. Clim Dyn. 2005 Mar 1;24(4):415–33.

54. Laridon Amaury. Development of a Simplified Dynamics Emulator and Investigation of Cascading Collapses of the AMOC and Greenland Ice Sheet in a Climate Model [Internet]. UCLouvain; 2024. Available from: https://dial.uclouvain.be/memoire/ucl/object/thesis:46552

55. Couplet V. Tipping cascades, future Earth system trajectories, and the prospect of a hothouse : a study with a reduced-complexity model. 2025.

56. Liu W, Xie SP, Liu Z, Zhu J. Overlooked possibility of a collapsed Atlantic Meridional Overturning Circulation in warming climate. Sci Adv. 2017 Jan 6;3(1):e1601666.

57. Smith CJ, Forster PM, Allen M, Leach N, Millar RJ, Passerello GA, et al. FAIR v1.3: a simple emissions-based impulse response and carbon cycle model. Geosci Model Dev. 2018 June 18;11(6):2273–97.